

First-Principles study of an $S = 1$ quasi-1D quantum molecular magnetic material

Maher Yazback, Jie-Xiang Yu, Shuanglong Liu, Long Zhang, Neil S. Sullivan, and Hai-Ping Cheng*
Department of Physics, University of Florida, Gainesville, Florida 32611, USA

(Dated: August 18, 2020)

We use density functional theory to study the structural, magnetic and electronic structure of the organo-metallic quantum magnet $\text{NiCl}_2\text{-4SC}(\text{NH}_2)_2$ (DTN). Recent work has demonstrated the quasi-1D nature of the molecular crystal and studied its quantum phase transitions at low temperatures. The system includes a magneto-electric (ME) coupling and, when doped with Br, the presence of an exotic Bose-glass state. Using the generalized gradient approximation (GGA) with inclusion of a van der Waals term to account for weak inter-molecular forces and by introducing a Hubbard U term to the total energy, we systematically show that our calculations reproduce the magnetic anisotropy, the inter-molecular exchange coupling strength and the magneto-electric effect in DTN, which have been observed in previous experiments. Further analysis of the electronic structure gives insight into the underlying magnetic interactions, including what mechanisms may be causing the ME effect. Using this computationally efficient model, we predict what effect applying an electric field might have on the magnetic properties of this quantum magnet.

I. INTRODUCTION

Interest in materials that exhibit sizable magneto-electric (ME) effects has grown considerably within the past decade. New classes of materials exhibiting the phenomena hint at applications where it can be harnessed, and materials can be designed for use in potential low-power spintronic devices¹ and future computing applications. The ME effect is characterized by a coupling between the magnetization and electric polarization of a material, that is, the application of a magnetic field induces a change in the electric polarization of a material and similarly, the application of an electric field causes a change in the magnetization. Investigations into the ME effect have largely focused on its presence within transition-metal oxides². Recent studies have shown that this coupling between the electric and magnetic properties may also be present within the class of materials known as organo-metallic molecular crystals².

The fundamental building block of these solids is a molecule where individual molecular units are held together by relatively weak inter-molecular interactions. At the center of each molecule is a magnetic metal ion, and the interactions between neighboring magnetic moments dictate the magnetic properties of the crystal. Given the weak interactions between molecules, molecular crystals are often easily strained under external magnetic and electric forces³. This soft lattice structure may provide a degree of freedom through which the ME effect may be tuned. The potential to synthesize organic ligands may also allow future flexibility in designing and tuning properties of such materials⁴.

The subject of this work is the organic quantum magnetic system dichloro-tetrakis-thiourea nickel, $\text{NiCl}_2\text{-4SC}(\text{NH}_2)_2$ (DTN),⁵ which has been studied in experiments and by quantum Monte-Carlo simulations based on model Hamiltonians^{2,3,6-10}. The molecular unit of this system (Figure I) has a central magnetic Ni cation surrounded by four electrically polar ligands, $\text{C}(\text{NH}_2)_2\text{S}$ (thiourea). DTN and its doped derivatives have been

studied extensively due to the rich physics present at low temperatures. The phase diagram^{2,3,7} of pure DTN shows that, at temperatures below 1.2K and below a critical magnetic field, H_{c1} , it is a quantum paramagnet. As the magnetic field, applied perpendicular to DTN's ab -plane, reaches the first critical field, it experiences a quantum phase transition into an XY -antiferromagnetic (XY -AFM) state where all spins now lie within the ab -plane. As the field is increased further the spins begin to cant, with a corresponding increase in magnetization. When a second critical field, H_{c2} , is reached, the magnetization saturates and the material enters a spin-polarized state where all spins are pointing along the c -axis and parallel to the applied magnetic field. Within this XY -AFM region DTN exhibits the ME effect where, along with an increase in magnetization, there is a correlated increase in the electric polarization. In this paper we investigate the structural, electronic and magnetic properties of DTN from first principles. Using appropriate levels of approximation within density functional theory^{11,12} (DFT) we are able to balance accurate structural predictions with computational efficiency to gain insight into DTN's electronic and magnetic structure, the possible mechanisms responsible for its ME effect, and investigate properties of the solid not yet studied in the literature.

The rest of the paper is organized as follows. Section II A presents an overview of the computational details involved in the calculations. Section II B discusses the theory behind modelling dispersion interactions and the approximations we made in attempting to obtain accurate structural properties. In section II C we discuss the addition of U_{eff} and the justification for our choice. In Section III we discuss our results relating to the systematic improvements made to our model, comparing to experiments along the way. Finally we go on to predict experimentally unverified properties of the material and summarize our conclusions in Section IV.

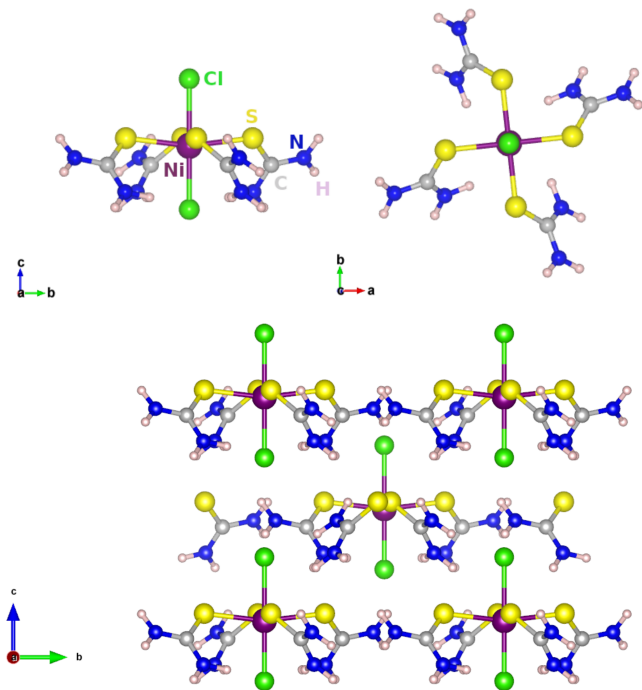


FIG. 1. (Top) Two views of the the molecular unit making up the DTN molecular crystal. Four thiourea ligands surround the magnetic Ni ion. (Bottom) The DTN unit cell.

II. METHODOLOGY

A. Overview

We performed first-principles calculations using the Vienna *ab initio* Simulation Package (VASP)^{13–15} within the density functional theory (DFT) framework.

The projector augmented wave pseudopotentials^{16,17} and generalized gradient approximations (GGA) of Perdew, Burke, and Ernzerhof¹⁸ were used for the exchange-correlation energy. To give an appropriate description of the on-site Coulomb interaction between Ni(*3d*) electrons, we apply the plus U method¹⁹ (GGA+ U) with $U_{\text{eff}} = U - J = 6.0$ eV on Ni when investigating the exchange couplings and the magnetic anisotropy of DTN. The D3²⁰ dispersion correction combined with GGA (GGA-D3) and/or GGA+ U (GGA-D3+ U) was used to take into account Van der Waals (vdW) interactions. The damping parameter for D3 was set to $S_R = 1.5$. Wavefunctions were expanded in plane waves and an energy cutoff of 520 eV was used for all calculations.

The Brillouin zone of the DTN unit cell containing two Ni^{2+} ions was sampled on a $6 \times 6 \times 6$ Monkhorst-Pack²¹ mesh for total energy and structure optimizing calculations with an applied Gaussian smearing of 0.01 eV. A $10 \times 10 \times 10$ Γ -centered K -mesh with the tetrahedron smearing method was used for the density-of-state (DOS)

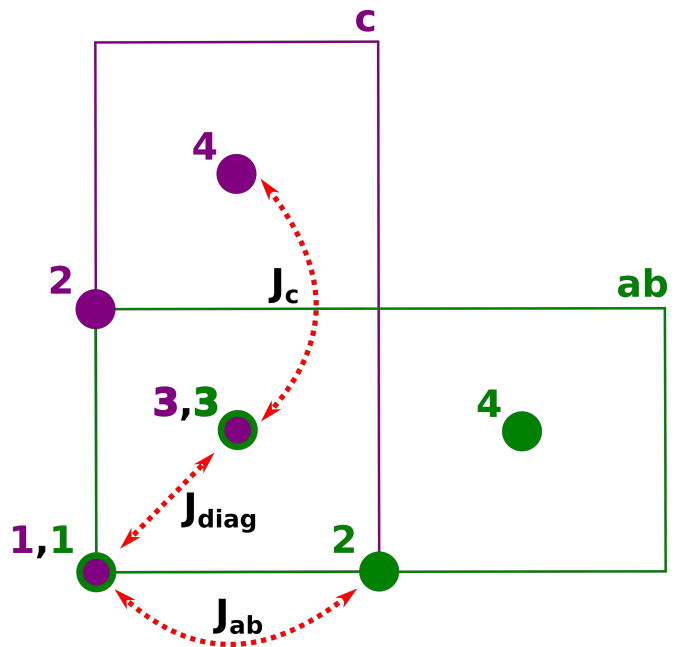


FIG. 2. The $2 \times 1 \times 1$ (ab , green) and $1 \times 1 \times 2$ (c , purple) supercells used to calculate respective exchange coupling J values. The nodes correspond to Ni ions and red arrows indicate the exchange interactions.

and orbital-resolved projected DOS (PDOS) calculation. The structure of DTN was relaxed for both the lattice constant and the atomic positions until atomic forces on each atom were converged to within 0.01 eV/Å.

Calculations of the exchange coupling J between magnetic Ni ions were performed by creating a supercell composed of two DTN unit cells with four Ni atoms, as shown in Figure 2. In order to compare to experiment, we focused on the J_c coupling along the c -axis of the unit cell and J_{ab} coupling between Ni ions within the ab -plane, or along the a/b axis. In addition, the J_{diag} coupling, which connects the corner Ni with the body-centered Ni ion was also considered. Two supercells, one of $1 \times 1 \times 2$ extending along c -axis and the other of $2 \times 1 \times 1$ extending along a/b -axis, were created to isolate inequivalent Ni ions. The corresponding K -mesh was therefore $6 \times 6 \times 2$ or $2 \times 6 \times 6$, respectively.

In order to gain insight into the magnetic interactions in DTN, we transformed the plane-wave-based Bloch states from VASP into Wannier function- (WF-) based local states by using the maximally-localized Wannier functions method²² implemented in the Wannier90 package²³. By choosing an initial guess of projections from the outer energy window, an effective tight-binding Hamiltonian \mathcal{H} was built in a downfolded Hilbert subspace where the eigenvalues in the inner energy windows are exactly the same as those of DFT results²⁴. Microscopic insights into the relevant orbitals and superexchange paths in DTN are based on the hopping integrals and on-site energies of the WF-based Hamiltonian, \mathcal{H} .

Magnetic anisotropy is a consequence of spin-orbit in-

interactions. We therefore performed non-collinear magnetic DFT calculations including spin-orbit interactions. We obtained the total energies for various configurations with each having a set of constrained directions of the local magnetic moments for the Ni atoms. The resulting total energy difference between configurations with moments perpendicular to one another gave the magnetic anisotropic energy. The direction with the lowest total energy is usually labeled as the easy axis.

B. Test of Van der Waals correction

TABLE I. Lattice constants of DTN with optimized structures obtained using different exchange-correlation functionals.

XC Functional	a (Å)	c (Å)
GGA	9.70	9.35
GGA-D3 ($S_R = 1.2$)	9.55	8.78
GGA-D3 ($S_R = 1.5$)	9.58	8.92
DF2	9.77	9.02
optB88	9.54	8.63
Experiment ⁵	9.56	9.08

Molecular crystals pose a challenge to theorist when trying to predict their structural properties. This has been especially true for GGA exchange-correlation functionals in DFT calculations, which struggle to account for long-range correlations like the Van der Waals (vdW) force²⁵ and hydrogen bonding. New functionals, optB88²⁶ and DF2²⁷, have been introduced recently to model these dispersive interactions accurately. In order to balance the computational cost of calculations while still accurately predicting molecular structures, we also consider the D3²⁰ dispersion correction, which is frequently cited for successfully predicting molecular crystal structures. The D3 dispersion adjusts the inter-nuclear energy to account for the long-range asymptotic behaviour with little effect at short range, giving an augmented DFT total energy.

We chose the vdW correction for our study after performing a benchmark test for the lattice constants of DTN. The DTN unit cell with two Ni atoms was used. The co-linear magnetic moments on the two magnetic Ni atoms in the unit cell are aligned anti-parallel. Structures were optimized for both lattice and atomic positions. The lattice constants for the DTN molecular crystal were investigated with various functionals and were compared with experimental data. The resulting tetragonal lattice constants, a and c , are listed in Table I. Without any vdW correction, both the lattice constants, a and c , are severely overestimated while using the GGA functional, the c lattice constant is especially, being 0.27 Å larger than the experimental value, indicating the failure to consider long-range vdW interactions with GGA.

Among the three vdW corrections GGA-D3, optB88 and DF2, optB88 underestimates lattice constants, especially c with a 0.45 Å difference compared to the experimental values. DF2 has small deviations, 0.21 Å for a and 0.06 Å for c , respectively, compared to the experimental values. GGA-D3 with the default value of damping parameter $S_R = 1.217$ overestimates the vdW interaction, so that it has a relatively large deviation of 0.30 Å for c , compared to the experimental value. GGA-D3 with a damping parameter $S_R = 1.5$ gives the best agreement with the experimental data. The deviation is only 0.02 Å for a and 0.16 Å for c . Considering that the D3 dispersion correction has less computational cost and performs better than optB88 and DF2, we employed GGA-D3 and GGA-D3+ U , with the adjusted damping parameter, for our future calculations on DTN. The lattice constants of DTN were set to $a = 9.58$ Å and $c = 8.92$ Å, the GGA-D3 result, for the rest of our calculations.

C. Estimation of U_{eff}

Constrained Random Phase Approximation (cRPA) calculations^{28,29} for the Ni site were carried out using the full-potential linearized augmented plane wave method implemented in the Exciting-Plus code³⁰ to have a reasonable estimate of the on-site Coulomb interaction of the Ni($3d$)-orbitals.

The basic idea of cRPA is to calculate a partial RPA particle-hole polarization with the constraint of a physically motivated correlation window, for example the d -like bands around the Fermi level. The on-site screened Coulomb interaction strength then can be determined from the partial RPA particle-hole polarization and the bare Coulomb interaction. The RPA polarization is obtained from Kohn-Sham susceptibility, which is completely based on the DFT ground state. We benchmarked it against other implementations using late transition metal monoxides and got consistent results³¹.

The molecular unit of DTN, as shown in Figure I, that was used has the Ni sitting in the center of the octahedron formed by four S atoms and two Cl atoms. A unit cell with bulk lattice constants but containing a single DTN molecule with 35 atoms in total was taken into account. This is enough for the calculation of the Kohn-Sham susceptibility and partial RPA polarization because the molecule is well separated from its nearest neighbors in the diagonal directions, and the feature of the strong interaction along the c -axis is preserved. The resulting diagonal elements of the U matrix, the on-site U , of d orbitals is ~ 4.9 eV and $J \sim 0.5$ eV. The cRPA calculation scheme is based on a paramagnetic ground state and magnetic properties of the material are not taken into account, so that the Pauli exclusion principle is not included in the calculation. This ignorance causes underestimation of the U values³¹. Thus, $U = 4.9$ eV is considered as a lower bound for the value of U_{eff} for our GGA-D3+ U calculations.

To further understand the influence of U_{eff} on the results of our GGA-D3+ U calculations, we calculated J_c , couplings along the c -axis, for various U_{eff} values. We used the structures obtained with the GGA-D3 functional for this benchmark test. The results are shown in Table II. The value of J_c for $U_{\text{eff}} = 4.9$ and $J = 0.52$ eV (calculated by cRPA) is -0.31 meV and for $U_{\text{eff}} = 4.9$ and $J = 0.0$ eV is -0.28 meV. The experimental value⁷ is -0.19 meV (-2.2 K) where the negative value corresponds to an antiferromagnetic coupling. This is a significant improvement over the GGA-D3 value of -1.05 meV. Since $U - J$ only adds a small correction, for the rest of the test we set $J = 0.0$ eV for simplicity: Then the values of J_c for $U_{\text{eff}} = 6.0$ and 7.0 eV are -0.21 and -0.16 meV, respectively. Considering the U_{eff} values used in the previous experimentally validated bulk NiO calculations^{19,32} and the results mentioned previously, we finally chose $U_{\text{eff}} = 6.0$ eV for our GGA-D3+ U calculations.

The U_{eff} -dependent magnetic anisotropy energies were also obtained with various U_{eff} values. The energy difference between spins along the c -axis and spins along a -axis is 0.78 – 0.79 meV (9.05 – 9.16 K) per unit cell for GGA-D3+ U with $U_{\text{eff}} = 4.9$ – 7.0 eV, indicating it is insensitive to U_{eff} . Here we set $J = 0$ eV. For completeness we calculated the magnetic anisotropy using $U = 4.9$ eV and $J = 0.52$ eV giving an anisotropy value within the $0.78 - 0.79$ meV window, which will be discussed again in Section III C.

III. RESULTS AND DISCUSSION

A. Structural properties

The Ni atoms in DTN form a body-centered tetragonal lattice so that there are two Ni atoms, one at the corner and the other at the body-center, in each tetragonal unit cell of DTN. Each Ni, with a +2 valence state, is surrounded by four S atoms in the ab -plane and two Cl atoms along the c -direction, leaving them in an octahedral crystal field. In each NiS_4Cl_2 octahedron, Cl atoms are located exactly on the apical sites along the c -axis, while S atoms in the polar thiourea ligands, $\text{C}(\text{NH}_2)_2\text{S}$, deviate a little from the ab -plane containing the central Ni.

A comparison of bond lengths and bond angles between the DFT relaxed structure using GGA-D3 and experiment⁵ is given in Table III. Bond lengths are all within 0.02 Å and bond angles are within 2.5° of the experimental values. This further confirms the consistency between the GGA-D3 approach and experiment.

B. Exchange coupling

Each magnetic Ni ion in molecular crystal DTN has spin $S = 1$. The tetragonal DTN bulk has two nonequivalent Ni-Ni spin couplings, one along the c -axis and an-

TABLE II. Average exchange coupling J^{avg} in units of meV along the c -axis and in the ab -plane using GGA and GGA+ U , compared to the experimental results,

XC	J_c^{avg}	J_{ab}^{avg}	J_{diag}
GGA-D3	-1.05	-0.149	-0.033
GGA-D3+ U (4.9)	-0.28	-0.023	-0.010
GGA-D3+ U (6.0)	-0.21	-0.018	-0.008
GGA-D3+ U (7.0)	-0.16	-0.015	-0.006
Experiment	-0.19	-0.016	N/A

TABLE III. Bond lengths and bond angles of structurally relaxed DTN using GGA-D3 compared to experiment.

Bond Length (Å)	Experiment	Calculated
Ni-Cl(1)	2.40	2.41
Ni-Cl(2)	2.52	2.54
Ni-S	2.46	2.44
S-C	1.73	1.72
C-NH ₂ (1)	1.34	1.34
C-NH ₂ (2)	1.32	1.33
Bond Angle (degrees)		
S-Ni-Cl(1)	96.7	96.8
S-Ni-Cl(2)	83.3	83.2
Ni-S-C	113.9	114.2
S-C-NH ₂ (1)	116.9	119.4
S-C-NH ₂ (2)	122.3	121.3
NH ₂ (1)-C-NH ₂ (2)	120.8	119.2

other in the ab -plane. The corresponding spin Hamiltonian in terms of Ni magnetic spins is

$$\mathcal{H}_s = -J_c \sum_{\langle i,j \rangle} S_i \cdot S_j - J_{ab} \sum_{\langle l,m \rangle} S_l \cdot S_m + D \sum_i (S_i^z)^2 - g\mu_B H \sum_i S_i^z \quad (1)$$

where $\langle i, j \rangle$ and $\langle l, m \rangle$ are the out-of-plane and in-plane neighbors, respectively, D is the coefficient of on-site uniaxial magnetic anisotropy, also known as the zero-field splitting, and $g\mu_B H$ is the interaction with an external magnetic field.

Experimentally it has been found that the exchange coupling J_c between Ni ions along the c -axis is an order of magnitude larger than the coupling J_{ab} within the ab -plane⁷. It is thus suggested that spins in DTN behave as quasi-1D spin chains. Therefore, we investigated the exchange coupling using the molecular crystal structures obtained from GGA-D3. As described in the methods section, the calculations for the exchange coupling J values involved creating two supercells, shown in Figure 2, extended along ab (green) and c directions (purple), to isolate the couplings of interest. We computed DFT total energies for various inequivalent spin configurations and

fit the exchange coupling J parameters to the Heisenberg model. Table II gives the calculated results for the exchange coupling J for GGA-D3 and GGA-D3+ U (with $U_{\text{eff}} = 6.0$ eV) compared to the experimental data. Both experiments and theory show that J_c is negative, an antiferromagnetic coupling, with strength an order of magnitude larger than J_{ab} .

Compared with the experimental value of -0.190 meV (-2.2 K), J_c with GGA-D3 is severely overestimated to be -1.05 meV (-12.2 K). The calculated J_{ab} is -0.149 meV (-1.73 K) using GGA-D3, which is also an order of magnitude larger than the experimental value -0.016 meV (-0.18 K). On the other hand, the GGA-D3+ U with the adjusted U_{eff} value gives results consistent with the experimental values for both J_{ab} and J_c . Although the two Ni ions are nearest neighbors, values of J_{diag} , the coupling between a corner Ni and a body-centered Ni, are even weaker than J_{ab} for both functionals. Because of the negligible values of both J_{ab} and J_{diag} , the strong J_c coupling makes DTN a quasi-1D antiferromagnetic chain along the c -axis.

Experiments suggest that strong exchange-coupling along the c -axis is via the Ni-Cl-Cl-Ni chain⁷. To examine the interatomic interactions, we investigated the electronic structure of the DTN unit cell with antiferromagnetic ordering. The resulting density of states (DOS) is shown in Figure 3. The total DOS in panel (a) shows that DTN is insulating, with a wide band gap of about 2.5 eV. In panel (b), the Ni $d_{3z^2-r^2}$ (red) and $d_{x^2-y^2}$ (blue) orbitals, often called e_g orbitals in an octahedral crystal field, are fully occupied in the spin-majority channel, and those in the spin-minority channel are almost fully empty, indicating a $S = 1$ spin state of the Ni²⁺ cation. In panels (d) and (e), Cl-Cl bonding and anti-bonding states are identified. The cross sections of the partial charge densities for these states are shown in panel (f). In the bonding state, an overlap between the two Cl(3p) ions appears, while there is a node between the two Cl ions in the anti-bonding state. The splitting between them is about 0.4 eV. The Cl-Cl distance is about 4.0 Å, much larger than the Cl-Cl bond length in Cl₂, and the energy splitting is smaller than typical $pp\sigma$ bond but is still much larger than the energy of the Van der Waals interaction. Therefore, it reflects strong inter-molecular interactions through the Cl-Cl chain along the c -axis. We note that Cl(3p) orbitals hybridize with the Ni($d_{3z^2-r^2}$) orbitals at about 0.5 eV below the Fermi level in the spin-up channel and about 3 eV above the Fermi level in the spin-down channel [Figure 3(b)(d)(e)]. In the plane of NiS₄ in the NiS₄Cl₂ octahedron, S atoms along S-Ni-S and along the a - and b -axes are labeled as S _{x} and S _{y} , respectively. In this case, S _{x} (p_x) and S _{y} (p_y) form σ bonds with Ni($d_{x^2-y^2}$) so that they are labeled as S($\sigma_{\text{S-Ni}}$) in panel (c). Just below the Fermi level, Ni($d_{x^2-y^2}$) hybridizes with S($\sigma_{\text{S-Ni}}$).

To understand the hybridization and the magnetic interaction pathway, we performed a unitary transformation on Bloch states to construct Wannier orbitals and

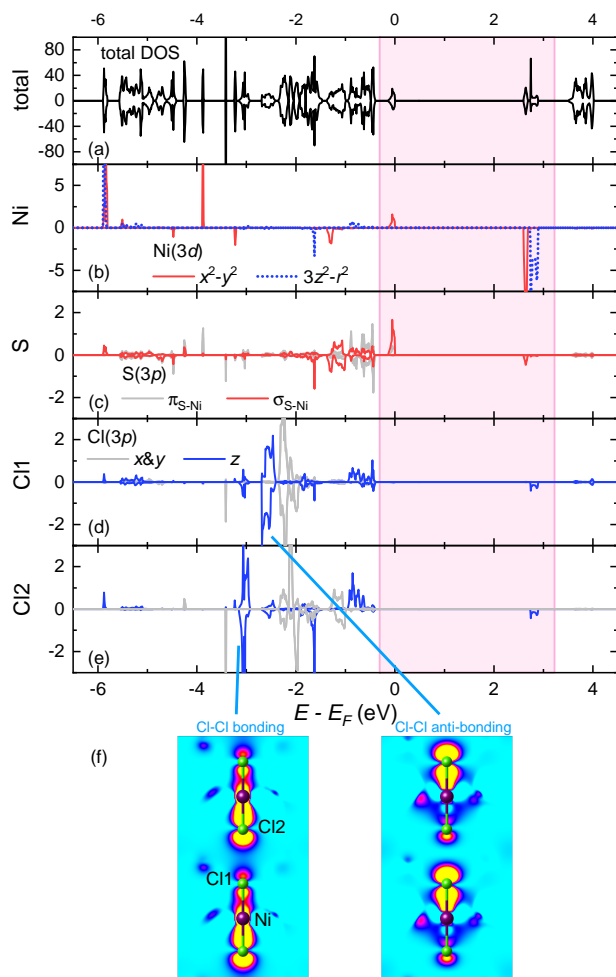


FIG. 3. Density of states (DOS) of the DTN unit cell using the GGA-D3+ U approximation. Panel (a) is the total DOS. Panels (b)–(d) are orbital-resolved projected DOS, or PDOS. Panel (b) shows $d_{3z^2-r^2}$ (red) and $d_{x^2-y^2}$ (blue) (e_g) orbitals of Ni(3d); (c) S 3p orbitals forming S-Ni σ bonds and π bonds respectively; and (d)(e) Cl(3p) orbitals of Cl1 and Cl2 identified in (f). Positive and negative values correspond to spin-majority and spin-minority channel, respectively. The Fermi level is set to zero. The shaded region is the inner energy window for constructing the Wannier-based tight-binding Hamiltonian. The cross section in a $1 \times 1 \times 2$ supercell in (f) shows the partial charge densities of Cl-Cl bonding and anti-bonding states labeled in (d)(e).

the tight-binding Hamiltonian. We used a $1 \times 1 \times 2$ supercell with antiferromagnetic coupling along the c -axis, and Ni(e_g) orbitals on each Ni ion were used as initial projections. In this case, a total of eight Wannier functions for each spin channel are localized exclusively on Ni ions.

The inner energy window we chose, from -0.25 to 3.2 eV, is shown in Figure 3. It covers both the valence and the conduction bands and so captures features of the gap for the virtual excitation in the exchange picture. The outer energy window covers all occupied states and

the unoccupied states below 5.0 eV.

The isosurface in Figure 4 shows one of the Wannier orbitals, which has features of $\text{Cl}(p_z)$, $\text{S}(\sigma_{\text{S-Ni}})$ and $\text{Ni}(e_g)$. These characteristics signal strong hybridization. The

corresponding matrix elements, in units of eV, including nearest-neighbor hopping t and the on-site energy ε in the WF basis, are

\mathcal{H}_{mn} (eV)	$ 1_{3z^2-r^2}^o\rangle$	$ 1_{x^2-y^2}^o\rangle$	$ 2_{3z^2-r^2}^u\rangle$	$ 2_{x^2-y^2}^u\rangle$	$ 3_{3z^2-r^2}^o\rangle$	$ 3_{x^2-y^2}^o\rangle$	$ 4_{3z^2-r^2}^u\rangle$	$ 4_{x^2-y^2}^u\rangle$
$\langle 1_{3z^2-r^2}^o $	-5.540	0.000	-0.031	0.000	0.000	0.023	0.000	0.000
$\langle 1_{x^2-y^2}^o $		-0.287	0.000	0.001	0.002	0.004	0.001	0.000
$\langle 2_{3z^2-r^2}^u $			2.570	0.000	0.005	-0.006	0.005	-0.008
$\langle 2_{x^2-y^2}^u $				2.405	-0.008	-0.002	-0.004	0.000
$\langle 3_{3z^2-r^2}^o $					-5.547	0.000	-0.031	0.000
$\langle 3_{x^2-y^2}^o $						-0.287	0.000	0.001
$\langle 4_{3z^2-r^2}^u $		<i>h.c.</i>					2.570	0.000
$\langle 4_{x^2-y^2}^u $								2.405

The position labels 1 to 4 of the WFs are the same as those in Figure 2. The subscripts $3z^2 - r^2$ and $x^2 - y^2$ represent the $3z^2 - r^2$ -like and $x^2 - y^2$ -like WFs centered on each Ni. Superscripts o and u refer to WFs with negative and positive on-site energies, respectively.

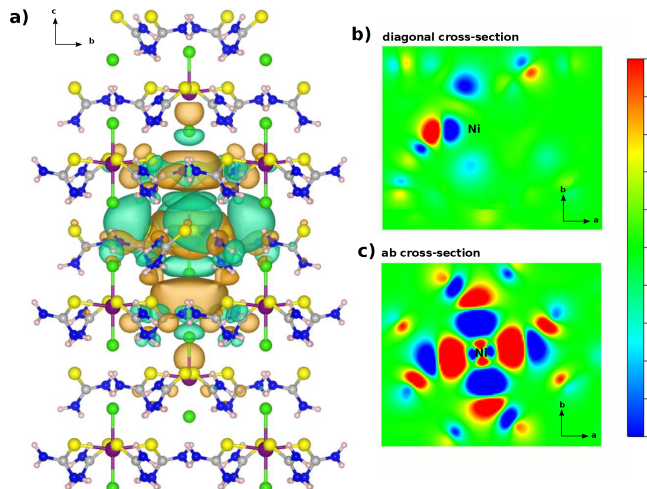


FIG. 4. (a) Isosurface of a Wannier function for the AFM c -axis supercell, indicating hybridization of Ni and Cl orbitals leading to a superexchange path along the Ni-Cl-Cl-Ni chain; (b) Wannier orbital in a cross section containing two Ni ions along a diagonal line of the lattice; and (c) in the ab plane of the lattice.

In particular, the largest hopping t between occupied and unoccupied WFs is -0.031 eV (indicated in bold in Eq. 2), which comes from two $3z^2 - r^2$ -like WFs of neighboring unit cells along the c -axis. Considering the difference in on-site energies, Δ , of associated WFs on Ni ions along the c -axis, we can estimate the magni-

tude of their exchange interaction by $J_c \sim 4t^2/\Delta$, to be about 0.474 meV (5.5 K). Other hopping elements between WFs centered on Ni ions with distinct occupied states are much smaller (around -0.001 eV or less), indicating a smaller exchange interaction along the diagonal direction and the a/b -axis directions. Overall, our results show that, although our estimate is of the right order of magnitude using a tight-binding model in the Wannier basis, using energetics and fitting to a Heisenberg model provides better J coupling values compared to experiment. An alternative WF-based Hamiltonian using atomic-centered projection [See Supplemental materials for details] further confirms the strong hopping between intermolecular $\text{Cl}(p_z)$ - $\text{Cl}(p_z)$ orbitals that plays a key role in the superexchange interaction. What we gain from our Wannier analysis³³ is more insight into the orbital contributions to the superexchange pathway.

C. Magnetic anisotropy

Besides the exchange coupling J , another important interaction in Eq. (1) is the magnetic anisotropy. To study the magnetic anisotropy in DTN, we performed spin-constrained DFT calculations including the spin-orbit interaction and non-collinear magnetic moments for both an isolated DTN molecule and a DTN molecular crystal. We first look at the isolated molecule, which is placed in a $20 \text{ \AA} \times 20 \text{ \AA} \times 20 \text{ \AA}$ supercell with adequate vacuum space, and only the Γ point in reciprocal space is calculated. The functional used in calculations is GGA-D3. By setting a series of constrained directions of Ni spin, the total energies $E(\theta, \phi)$ as a function of direction angles are obtained. In the crystal unit cell with two Ni atoms, the corner Ni spin is fixed to be aligned along the c -axis and a different spin direction for the body-

centered Ni is sampled using spherical coordinates. The resulting relative energy maps for $E(\theta, \phi)$ are shown in Figure 5. In the case of a single DTN molecule, the lowest energy is at $\theta = 90^\circ$, the in-plane direction, and the highest energies are at $\theta = 0^\circ$ and 180° , when the spins are along the c -axis. Since the energy as a function of ϕ is almost invariant, this indicates that the ab -plane is the easy axis, with little ϕ dependence, and the c -axis is the hard axis. The energy difference $E(0^\circ, \phi) - E(90^\circ, \phi)$ is 0.20 meV (2.32 K). This result shows a uniaxial magnetic anisotropy of the DTN molecule. For the molecular crystal, $E(0^\circ, \phi)$ is the highest while $E(180^\circ, \phi)$ is the lowest. The energy difference $E(0^\circ, \phi) - E(180^\circ, \phi)$ is 0.59 meV (6.84 K). Since the spin of the corner Ni is fixed along the c -axis, the direction of the central Ni spin with lowest energy corresponds to antiferromagnetic spin-ordering with the corner Ni spin.

The definition of D , the zero-field splitting, is the energy difference between states with $S_z = \pm 1$ and $S_z = 0$ for an $S = 1$ system. DFT calculations can only give the quantum state $S_x = \pm 1$, instead of $S_z = 0$, when the spin is constrained along a -axis. To calculate the magnetic anisotropy for the unit cell with two Ni atoms, we take the energy difference between configurations where the spins in one configuration are aligned along the c -axis and along the a -axis for the other configuration. The energy difference $E(0^\circ, \phi) - E(90^\circ, \phi)$ per Ni by DFT is just half the magnitude of D . Therefore, $D = 2[E(0^\circ, \phi) - E(90^\circ, \phi)]$ for DTN. The experimental value is $D = 0.774$ meV (8.98 K).

For the DTN crystal, we performed both GGA-D3 and GGA-D3+ U with $U_{\text{eff}} = 6.0$ eV. Using the GGA-D3 functional, we underestimate D to be 0.54 meV (6.26 K). A GGA-D3+ U calculation gives $D = 0.78$ meV (9.10 K), consistent with the experimental results. We also examined $U = 7.0$ eV and $U - J$ with $U = 4.9$ eV and $J = 0.52$ eV calculated by cRPA and found that D is insensitive corresponding to a D value of 0.78 meV for both. It is worth noting that for heavy elements that involve f electrons, a nonspherical $U - J$ scheme may be needed³⁴.

A fuller investigation of magnetic anisotropy, including the effects of substitutions of Cl ions and ligands, will be left for future work. Earlier results suggest a decrease in magnetic anisotropy as the substitute ion gets larger³⁵.

D. Magneto-electric effect

With an understanding of the magnetic interactions in DTN we turn to the magneto-electric (ME) effect. To investigate this effect we again performed spin-constrained DFT calculations, including the spin-orbit interaction and non-collinear magnetic moments. This was done for the DTN molecular crystal with two Ni atoms and using the GGA-D3 functional and its corresponding relaxed structure. Constraining the moment direction of each Ni relative to the c -axis allowed us to simulate what mag-

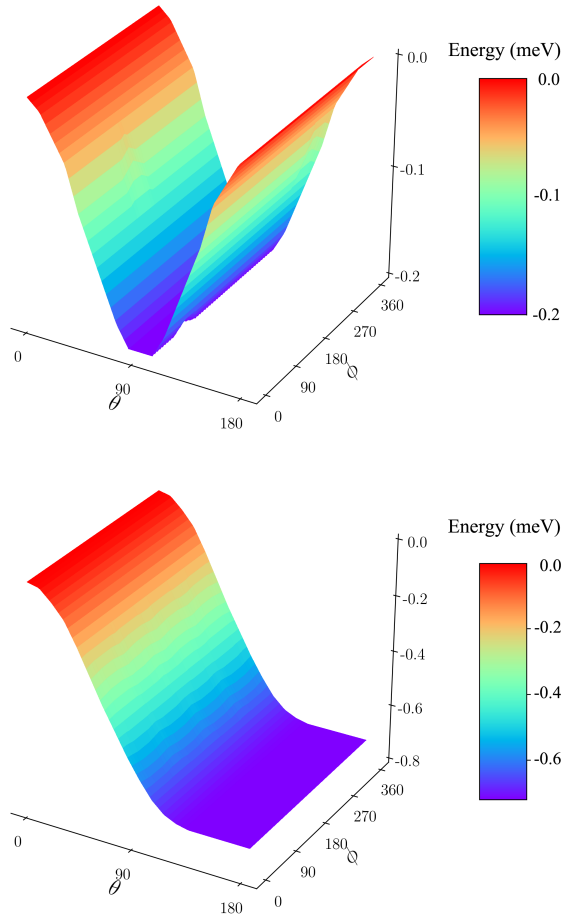


FIG. 5. Relative total energy as a function of the angle between the c -axis and the spin of the Ni ion for (Top) the DTN molecule and (Bottom) the DTN unit cell with the other inequivalent Ni ion spin fixed along the c -axis. The angles θ and ϕ refer to the orientation angles in spherical coordinates.

netic configurations would result when a magnetic field is applied parallel to the c -axis of the molecular crystal. The spin canting angle in Figure 6 is equivalent to the polar angle relative to the c -axis. A spin-canting angle of 0° corresponds to spins that are parallel to the c -axis and representing the spin-polarized state at high magnetic fields. Similarly, a 90° angle corresponds to spins lying in the ab -plane and the XY-AFM state. For each configuration we calculated the electric dipole moment of the crystal within the modern theory of polarization framework³⁶. What we see in Figure 6 is that as the canting angle θ increases and the spins approach the ab -plane, there is a correlated decrease in the electric dipole moment (blue) of the crystal together with the expected decrease in M_z (red). This indicates the presence of an ME coupling within the DTN molecular crystal.

To probe the mechanism responsible for the ME coupling we investigate what effect straining the molecular

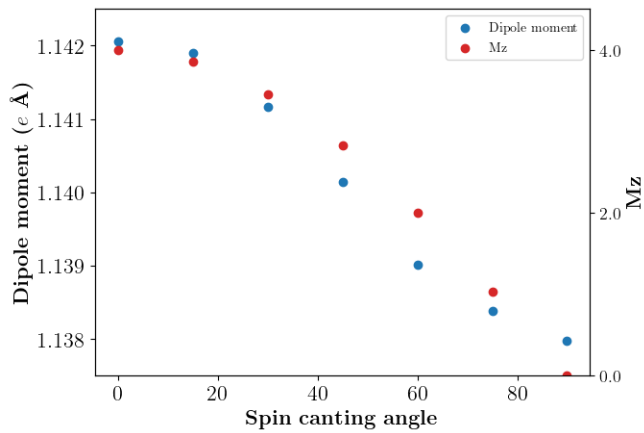


FIG. 6. Magneto-electric coupling in DTN. The electric dipole moment (blue) and the z -component of the magnetization (red) are plotted as a function of the spin canting angle of the spin moment on the Ni cation.

crystal has on the electronic polarization. The literature suggests magnetic field-induced strain, *i.e.* magnetostriction, changes the unit cell and a reorientation of the electrically polar ligands may be responsible for the change in polarization³. To test this, we used the DTN molecular crystal and the GGA-D3 functional structures from our ME calculations with collinear spins in an AFM configuration and no spin-orbit interaction. We applied a tensile strain on the DTN unit cell along the c -axis of up to 0.1% while correspondingly compressing the a , b lattice constants, keeping the volume constant, and allowed the ions to relax to minimize the total energy. Similarly, we applied a compression to the c lattice constant while expanding the a , b constants. We calculated the polarization as a function of applied strain. We distinguish the change in polarization relative to the unstrained system, ΔP , resulting from ionic motion (blue) from that due to changes in electronic density (green) in Figure 7. The results indicate that the main contribution to the change in polarization comes from subtle changes in electronic density rather than a reorientation of the thiourea ligands. An analysis of the molecular crystal structure shows little variation in the Cl-Ni-S bond angles or bond lengths, supporting this result.

To conclude our study of the ME effect in DTN, we investigate what effect applying an electric field has on the magnetic properties of the molecular crystal. Specifically, we investigate the magnetic anisotropy (MAE) as a function of electric field strength where the electric field is aligned parallel to the a -axis and perpendicular to the 1D-chain. In these calculations we used the DTN molecular crystal unit cell structure with two Ni atoms and the GGA-D3+ U exchange-correlation functional with $U_{\text{eff}} = 6$ eV. As with our previous MAE calculations, we performed noncollinear magnetic DFT calculations including spin-orbit interactions and obtained the energy difference between two configurations of spins

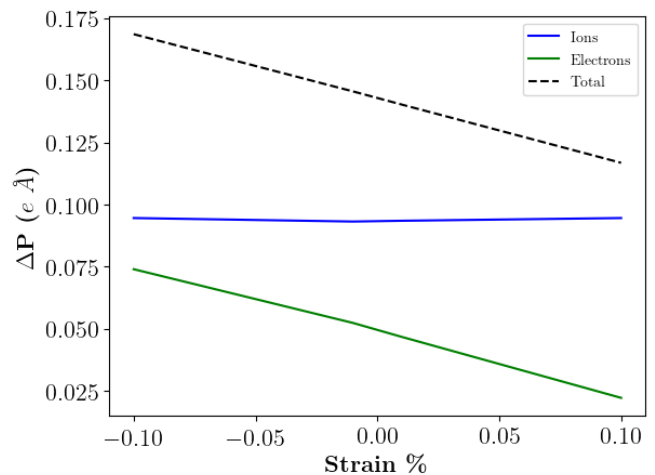


FIG. 7. Ionic and electronic contributions to the change in polarization of the DTN unit cell under applied strain.

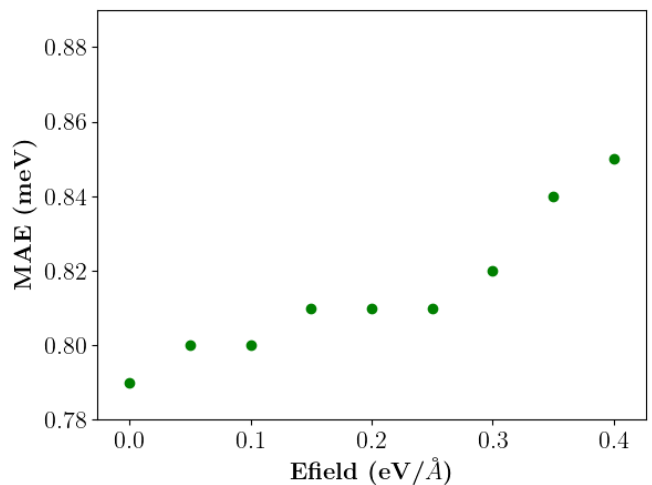


FIG. 8. The dependence of the magnetic anisotropy of bulk DTN on an electric field applied parallel to the ab -plane.

aligned 90° relative to one another. The results show that by increasing the strength of the electric field, we are able to increase the MAE of bulk DTN (Figure 8). This indicates the presence of a reverse coupling in this molecular crystal, not observed experimentally, showing that the magnetic properties may be tuned by electronic means.

IV. CONCLUSION

Our aim in this paper has been an attempt to model DTN within a DFT framework. This approach not only provides a way to gain insight into the mechanisms responsible for structural, electronic and magnetic properties, but also allows us to make accurate predictions while minimizing the computational cost. We were able

to show that the inclusion of the GGA-D3 correction substantially improves the structure of the DTN molecular crystal, providing accurate lattice constants, bond lengths and bond angles. Adding the Hubbard term to the standard GGA functional allowed us to improve our modelling of the magnetic interactions in DTN, accurately predicting the magnetic anisotropy and exchange coupling constants and providing an additional J_{diag} coupling. The quasi-1D nature of DTN was indicated by the hybridization of $\text{Ni}(d_{3z^2-r^2})$ and Cl-Cl anti-bonding orbitals via a virtual superexchange path along the c -axis. Finally, we showed the presence of a ME coupling and predict an increase in magnetic anisotropy with the application of an electric field. The results of this study are a first step towards understanding the detailed mechanisms involved in the magneto-electric coupling in DTN.

Its presence in functional organic quantum magnets suggests the possibility of future applications where the magnetic properties of materials may be fine-tuned through more feasible structural and electronic means. Yet to be explored in detail is the nature of Bose-Einstein condensates (BEC) in organic quantum magnets⁷ and the important role the ME effect plays in this state. We hope this work puts forward the idea that these fundamental properties may be investigated from first principles.

Acknowledgments: This work was supported as part of the Center for Molecular Magnetic Quantum Materials, an Energy Frontier Research Center funded by the U.S. Department of Energy, Office of Science, Basic Energy Sciences under Award No. DE-SC0019330. Computations were performed at NERSC and UFR.

-
- * hping@ufl.edu
- ¹ S. Fusil, V. Garcia, A. Barthélémy, and M. Bibes, *Annual Review of Materials Research* **44**, 91 (2014).
 - ² V. Zapf, F. Wolff-Fabris, M. Kenzelmann, F. Nasreen, F. Balakirev, Y. Chen, and A. Paduan-Filho, in *Journal of Physics: Conference Series*, Vol. 273 (IOP Publishing, 2011) p. 012132.
 - ³ V. Zapf, V. Correa, P. Sengupta, C. Batista, M. Tsukamoto, N. Kawashima, P. Egan, C. Pantea, A. Migliori, J. Betts, *et al.*, *Physical Review B* **77**, 020404 (2008).
 - ⁴ O. Sato, *Nature chemistry* **8**, 644 (2016).
 - ⁵ A. Lopez-Castro and M. R. Truter, *Journal of the Chemical Society (Resumed)*, 1309 (1963).
 - ⁶ E. Mun, J. Wilcox, J. L. Manson, B. Scott, P. Tobash, and V. S. Zapf, *Advances in Condensed Matter Physics* **2014** (2014).
 - ⁷ R. Yu, L. Yin, N. S. Sullivan, J. Xia, C. Huan, A. Paduan-Filho, N. F. Oliveira Jr, S. Haas, A. Steppke, C. F. Miclea, *et al.*, *Nature* **489**, 379 (2012).
 - ⁸ A. Orlova, R. Blinder, E. Kermarrec, M. Dupont, N. Laflorie, S. Capponi, H. Mayaffre, C. Berthier, A. Paduan-Filho, and M. Horvatić, *Physical Review Letters* **118**, 067203 (2017).
 - ⁹ M. Dupont, S. Capponi, M. Horvatić, and N. Laflorie, *Physical Review B* **96**, 024442 (2017).
 - ¹⁰ A. Paduan-Filho, *Brazilian Journal of Physics* **42.3-4**, 292 (2012).
 - ¹¹ P. Hohenberg and W. Kohn, *Physical Review* **136**, B864 (1964).
 - ¹² W. Kohn and L. J. Sham, *Physical Review* **140**, A1133 (1965).
 - ¹³ G. Kresse and J. Furthmüller, *Phys. Rev. B* **47**, 558 (1993).
 - ¹⁴ G. Kresse and J. Furthmüller, *Computational materials science* **6**, 15 (1996).
 - ¹⁵ G. Kresse and J. Furthmüller, *Physical Review B* **54**, 11169 (1996).
 - ¹⁶ P. E. Blöchl, *Physical Review B* **50**, 17953 (1994).
 - ¹⁷ G. Kresse and D. Joubert, *Physical Review B* **59**, 1758 (1999).
 - ¹⁸ J. Perdew, K. Burke, and M. Ernzerhof, *Errata:(1997) Phys Rev Lett* **78**, 1396 (1996).
 - ¹⁹ S. Dudarev, G. Botton, S. Savrasov, C. Humphreys, and A. Sutton, *Physical Review B* **57**, 1505 (1998).
 - ²⁰ S. Grimme, S. Ehrlich, and L. Goerigk, *Journal of computational chemistry* **32**, 1456 (2011).
 - ²¹ H. J. Monkhorst and J. D. Pack, *Physical Review B* **13**, 5188 (1976).
 - ²² N. Marzari and D. Vanderbilt, *Physical Review B* **56**, 12847 (1997).
 - ²³ A. A. Mostofi, J. R. Yates, Y.-S. Lee, I. Souza, D. Vanderbilt, and N. Marzari, *Computer physics communications* **178**, 685 (2008).
 - ²⁴ I. Souza, N. Marzari, and D. Vanderbilt, *Physical Review B* **65** (2001), 10.1103/physrevb.65.035109.
 - ²⁵ L. Kronik and A. Tkatchenko, *Accounts of chemical research* **47**, 3208 (2014).
 - ²⁶ J. Klimeš, D. R. Bowler, and A. Michaelides, *Journal of Physics: Condensed Matter* **22**, 022201 (2009).
 - ²⁷ K. Lee, É. D. Murray, L. Kong, B. I. Lundqvist, and D. C. Langreth, *Physical Review B* **82**, 081101 (2010).
 - ²⁸ F. Aryasetiawan, M. Imada, A. Georges, G. Kotliar, S. Biermann, and A. I. Lichtenstein, *Physical Review B* **70**, 195104 (2004).
 - ²⁹ F. Aryasetiawan, K. Karlsson, O. Jepsen, and U. Schönberger, *Physical Review B* **74**, 125106 (2006).
 - ³⁰ A. Kozhevnikov, A. G. Eguiluz, and T. C. Schulthess, in *2010 ACM/IEEE International Conference for High Performance Computing, Networking, Storage and Analysis (IEEE, 2010)*.
 - ³¹ L. Zhang, P. Staar, A. Kozhevnikov, Y.-P. Wang, J. Trnastic, T. Schulthess, and H.-P. Cheng, *Physical Review B* **100** (2019), 10.1103/physrevb.100.035104.
 - ³² T. Cai, H. Han, Y. Yu, T. Gao, J. Du, and L. Hao, *Physica B: Condensed Matter* **404**, 89 (2009).
 - ³³ A. E. Thuijs, X.-G. Li, Y.-P. Wang, K. A. Abboud, X.-G. Zhang, H.-P. Cheng, and G. Christou, *Nature communications* **8**, 500 (2017).
 - ³⁴ F. Zhou and V. Ozolins, *Physical Review B* **80**, 125127 (2009).
 - ³⁵ J. Gu, S. Liu, M. Yazback, H.-P. Cheng, and X.-G. Zhang, *Physical Review Research* **1**, 033183 (2019).
 - ³⁶ R. King-Smith and D. Vanderbilt, *Physical Review B* **47**, 1651 (1993).